Pyrophosphonate Covalent Organic Frameworks

Xu Ke,[‡1] Robert Oestreich,[‡2] Takin Haj Hassani Sohi,[‡2] Mailis Lounasvuori,[3] ,Jean G. A.Ruthes,[4,5] Yunus Zorlu,[6] Philipp Seiffert,[2] Till Strothmann,[2] Patrik Tholen,[7] Markus Suta,[2] Volker Presser,[4,5] Tristan Petit,[3] Christoph Janiak,[2] Jens Beckmann,[8] Jörn Schmedt auf der Günne[1], Gündoğ Yücesan[2]**

1. Department of Chemistry and Biology, Inorganic Materials Chemistry, University of Siegen, Adolf-Reichwein-Straße 2, 57076 Siegen, Germany
2. Institut für Anorganische Chemie und Strukturchemie, Heinrich-Heine-Universität Düsseldorf, Universitätsstraße 1, 40225 Düsseldorf, Germany
3. Young Investigator Group Nanoscale Solid-Liquid Interfaces, Helmholtz-Zentrum Berlin für Materialien und Energie GmbH, Albert-Einstein-Straße 15,12489 Berlin, Germany
4. INM – Leibniz Institute for New Materials, Campus D22, 66123 Saarbrücken, Germany.
5. Department of Materials Science and Engineering, Saarland University, Campus D22, 66123 Saarbrücken, Germany.
6. Department of Chemistry, Gebze Technical University, Kocaeli, Türkiye.
7. Technische Universität Berlin, Lebensmittelchemie und Toxikologie, Gustav-Meyer-Allee 25, 13355 Berlin, Germany
8. Institut für Anorganische Chemie und Kristallographie, Universität Bremen, Leobener Str. 7, Bremen 28359, Germany

Keywords:

Covalent Organic Frameworks; Pyrophosphonate Linkages; Carbon Capture; Stable COFs

Abstract

Herein, we report a new family of covalent organic frameworks (COFs), namely pyrophosphonate-COFs, constructed via pyrophosphonate linkages. Pyrophosphonate-COFs can be synthesized via a single-step condensation reaction of the charge-assisted hydrogen-bonded organic framework (HOF) GTUB5, which is constructed from phenylphosphonic acid and 5,10,15,20-tetrakis[p-phenylphosphonic acid] porphyrin. The reported pyrophosphonate-COF, which we call GTUB5-COF was synthesized by simply heating its two-linker HOF precursor GTUB5 without using chemical reagents. GTUB5-COF exhibits good water and water vapor stability during the gas sorption measurements. Furthermore, GTUB5-COF exhibits exceptional electrochemical stability in 0.5 M Na_2SO_4 electrolyte in water. The formation of pyrophosphonate bonds upon heating was confirmed by magic angle spinning nuclear magnetic resonance spectroscopy, Fourier-transform infrared spectroscopy, and mass spectrometry coupled with thermal analysis. The condensed product pyrophosphonate-COF can efficiently adsorb CO_2. It has a more favorable heat of adsorption value for CO_2 capture at lower pressures than water vapor, making it a suitable candidate for selective CO_2 capture in the presence of water vapor. The absorption and emission of GTUB5-COF are governed by localized transitions (Soret and *Q* bands) within the porphyrin unit, which results in broad-banded fluorescence in the near-infrared range at around 800 nm.

Introduction: Covalent organic frameworks (COFs) are sister compounds of metal-organic frameworks (MOFs) and hydrogen-bonded organic frameworks (HOFs).[1-3] COFs are synthesized via the covalent linkage of organic building blocks to form two or three-dimensional microporous frameworks.[4] Since the first report of on boroxine-linked COFs in 2005,[2] COF research has been a very active research area due to their tunable porosity and potential for pore functionalization via organic linker design or post-synthesis modifications.[5] To date, many different COF families have been reported in the literature based on their covalent linkage. COFs can be synthesized through a wide range of reactions, including condensation reactions (i.e., boroxine linkage), Schiff base reactions (i.e., imine, hydrazone, enamine, phenazine linkages), click reactions (i.e., triazole linkage), metal-catalyzed coupling reactions (i.e., C-C linkages), etc.[6-10] The thermal and chemical stability and permanent porosity observed in some COF families opened many potential applications such as gas storage, water adsorption, catalysis, water harvesting, CO_2 capture, catalysis, photocatalysis, semiconductors, energy storage, luminescence.[6, 11-16]

Recently, we have reported on the synthesis of hydrogen-bonded organic frameworks constructed using arylphosphonic acids.[17, 18] Due to their short hydrogen bond distances around 2.5 Å (bonds shorter than 2.4 Å of donor oxygen-acceptor oxygen pair (O-O) distances involved in hydrogen bonds are considered to have near covalent bond strength up to 50 kJ/mol bond dissociation energy[19]) and formation of multiple hydrogen bonds between the arylphosphonic acid linkers, these HOFs exhibited exceptional stability at 90 °C and 90% relative humidity (RH) and after proton conductivity experiments at 75 °C and 75% RH. Other groups also reported the exceptional stability of phosphonic acid HOFs after proton conduction.[20] Our recent unit cell checks on the first batch of GTUB-5 (derived from phenylphosphonic acid and 5,10,15,20-tetrakis[p-phenylphosphonic acid] porphyrin) crystals are still providing the same unit cell after 4 years of storage at room temperature and ambient humidity. In the literature, arylphosphonic acids resist thermal decomposition, hydrolysis, and decomposition under UV light.[21] Expectations on pyrophosphonate-COFs that are synthesized after condensation of phosphonic acid HOFs are high stability and high structural versatility. They are also expected to generate flexible pores due to flexible sp^3 P-O-P bonds. Such flexible and stable microporous platforms have the potential to spawn realistic industrial applications to capture gases selectively.

Jessen's group has recently shown that branched inorganic pyrophosphates exhibit good stability in water.[22] Hypothetically, organic pyrophosphonates are expected to create better stability compared to inorganic pyrophosphates. Furthermore, phosphonate esters are cleaved in the presence of 37% HCl under reflux conditions to form the corresponding phosphonic acids, indicating their stability in acidic environment.[23] There is limited information in the literature about the condensation of phosphonic acids. For example, there are a few reports about the ab initio calculations studying the condensation of phosphinic acids and methylphosphonic acid to provide geometry and reaction energies to form dimers, trimers, tetramers and cyclization.[24, 25] There are also limited experimental reports in the literature reporting the condensation of phosphonic acid to form dimers. For example, a proton-conducting polymer poly(vinyl phosphonic acid) is known to condense forming dimers at higher temperatures, which limits its proton-conducting ability. There is another study by Yücesan et al. that reports the crystal structure of solvothermally condensed phenyl phosphonic acid in acetonitrile at 150 °C, at which the respective product generates a metallomacrocycle with Cu(II) ions and 2,2'-bipyridine.[26] A similar work was also reported later by Zheng using Ag(I) ions.[27, 28] The other reports in the literature about forming pyrophosphonate dimers, trimers or macrocycles were synthesized chemically, such as ring-opening polymerization of cyclic phosphonates.[29] In this work, we used our previously reported charge-assisted HOF GTUB5 as the model system to form the first pyrophosphonate-COF after condensation of phosphonic acids, phenylphosphonic acid and 5,10,15,20-tetrakis[p-phenylphosphonic acid] porphyrin using a simple heating in the literature (**Scheme 1**). Herein, we report the structural characterization of the first pyrophosphonate-COF, and we explore its thermal, chemical, and electrochemical stability, CO_2 capture, and optical properties.

Synthesis and characterization of pyrophosphonate bonds: As seen in **Scheme 1**, the donor-acceptor O-O distances between hydrogen-bonded phosphonic acid moieties of GTUB5 is ca. 2.5 Å (hydrogen bonds with shorter donor-acceptor O-O distances than 2.4 Å can have high bond dissociation energies up to 50 kJ/mol; for more detailed information about the hydrogen bond lengths in phosphonic acids, see references [30] and [18]).[19] Therefore, the phosphonic acid groups in GTUB5 crystals are already aligned in a favorable position to initiate the condensation reaction.[18, 30] Furthermore, the charge-assisted hydrogen-bonded network of GTUB5 with the presence of fully deprotonated phenylphosphonic acid moieties and DMA^+

(dimethylammonium cations) could hypothetically help promote the condensation reaction following the nucleophilic substitution on 5,10,15,20-tetrakis[p-phenylphosphonic acid] porphyrin and fully deprotonated phenylphosphonic acid phosphorus atoms. Thermogravimetric analysis (TGA) coupled with mass spectrometry (MS) of GTUB5 and FT-IR suggests condensation of HOF begins after ca. 130 °C due to evaporation of water and continues until ca. 230 °C. The solid crystals of GTUB5 were heated gradually in oven to 230 °C to promote the condensation of phosphonic acids to form pyrophosphonate bonds. The crystals retained their initial color and shape after heating to 230 °C. Despite the crystalline look of the final product GTUB5-COF (*Supporting Information*), single crystal diffraction didn't provide reflections suitable for data collection.

Characterization of pyrophosphonate bonds via MAS NMR: Due to the low crystallinity of the material, we used solid-state ^{1}H, ^{13}C, and ^{31}P NMR spectroscopy to observe the structural changes between the arylphosphonic acid linkers in GTUB5 after annealing. Magic angle spinning (MAS) NMR experiments were performed with 7.04 T magnet spectrometer with Topspin V4.0.5, operating at the frequencies of 121 MHz for ^{31}P, respectively (See SI for more experimental details. The peaks observed in the ^{1}H and ^{13}C MAS NMR spectra of both untreated HOF GTUB5 and the annealed GTUB5-COF (**Figure S1-S2**, *Supporting Information*) were successfully assigned to their corresponding environments (**Figure S3**, **Table S1-S2**, *Supporting Information*). These results confirm that no decomposition reactions are happening within the organic moieties of GTUB5 after annealing to 220 °C. The ^{31}P MAS spectra show that the peaks of the untreated crystalline GTUB-5 (starting material) broaden gradually at higher temperatures, and a second peak at 5 ppm steadily emerges as the sample is heated to 220 °C (**Figure 1-2**). In the case of inorganic phosphate salts, condensation to form pyrophosphate bonds is recognized to induce a shift in resonances, typically shifting them by approximately 10 ppm and lower values.[31, 32] The characterization of protonated phosphates is more complicated due to the more substantial influence of the hydrogen-bonded protons.[33, 34] To the best of our knowledge, there is no similar correlation tool for phosphonate ^{31}P shifts. Therefore, we gathered the isotropic chemical shift values for monophosphonates and pyrophosphonates compiled from the literature (**Table 2, Figure 3**).[31, 32] A similar trend as for phosphate groups can also be seen for phosphonate groups. Still, there is a significant amount of overlap between the chemical shift ranges for mono- and pyrophosphonate groups. The anisotropic chemical tensor was investigated for differences in the chemical shift anisotropy

(**Table 1**). However, similar to hydrogen-phosphates, the hydrogen-bonded protons strongly influence the chemical shift tensor, and only insignificant differences were observed.

A more reliable tool to distinguish pyrophosphonates from phosphonic acids is magnetic dipole-dipole coupling between neighboring P atoms. The condensation of the R-PO_3H_2 moieties in GUTB-5 to form R-P(O)(OH)-O-P(O)(OH)-R (**Scheme 1**) moieties upon annealing can be tested by measuring the distances between neighboring P atoms using this method. In a P-O-P bridge, as in a pyrophosphonate group, the shortest P-P distances can be estimated to be of the order of 300 pm,[27, 28] while in monophosphonates, the minimum distance would amount to about 460 pm.[35, 36] The dipole-dipole coupling relates to the inverse cubic internuclear distance. Therefore, the P-P distances in two-spin-systems can be estimated from the magnetic dipole-dipole coupling, for example, by ^{31}P-^{31}P double-quantum NMR experiments with an error of about 10%, including effects by the anisotropic J-coupling. [37] To this end, a homonuclear ^{31}P-^{31}P double-quantum constant-time (DQCT) experiment was conducted, in which the peak at 5 ppm under the chosen conditions shows no zero-crossing while the peak at 15 ppm does (**Figure 4**).[38] Based on these observations, the two peaks were unambiguously assigned to pyrophosphonate and monophosphonate groups, respectively, which means the annealing to 220 °C only led to a partial condensation.

Double-quantum constant-time (DQCT) conversion curves with well-expressed zero-crossings (**Figure S4**, *Supporting Information*), as in this case, can be analyzed for the magnetic dipole-dipole coupling by fitting the experimental data in a two-spin approximation (**Figure 5**), which for the pyrophosphonate is a good approximation because further spins are significantly farther away.[38] The analysis revealed a dipole-dipole coupling of $\nu_{P\text{-}P}$ = –828 Hz for the signal at δ = 5 ppm, corresponding to a P-P distance of $r_{P\text{-}P}$ = 2.9 Å within the pyrophosphonate group. The bond length includes a small uncertainty of around 10% for the effective coupling constant caused by the anisotropic $^2J(^{31}P,^{31}P)$-coupling, translating into an error of about 0.1 Å. It can be concluded that the presence of a pyrophosphonate group can be unambiguously evidenced by solid-state NMR.[37]

Characterization of pyrophosphonate bonds via FTIR: The condensation of HOF GTUB5 to GTUB5-COF at higher temperatures was monitored with temperature variable FTIR spectroscopy. First, the sample was heated to 50 °C, and a spectrum was recorded. Then, the sample was evacuated at 50 °C overnight. This resulted in increased transmittance at 3400 and 1635 cm^{-1}, indicating a loss of water, either structural water incorporated in the HOF or contamination in the KBr used to prepare the pellet (**Figure S5***, Supporting Information*).

Then, the sample was maintained in a vacuum as the temperature was increased (**Figure 6a**). As the sample was heated, increased transmittance was observed at 2700 cm^{-1}, 2450 cm^{-1}, 1710 cm^{-1}, and 1050 cm^{-1}, and assigned to the loss of phosphonic acid groups.[39-43] Decreased transmittance at 970 cm^{-1} was assigned to forming P-O-P linkages.[44] The P-O-H deformation mode in a phosphonic acid is also expected to absorb at around 960 cm^{-1}.[40, 42] Difference spectra (**Figure 6b**) show a bipolar band at this frequency range, supporting the conclusion that phosphonic acid groups are condensing to form pyrophosphonate linkages. Similarly, difference spectra show a bipolar band around 1230 cm^{-1} where the P=O bond in both phosphonic acid and pyrophosphonate absorbs, and the condensation or the phosphonic acid groups results in a subtle change in the vibrational frequency of the P=O bond.[39-44]

Thermal and chemical stability: The thermal stability of GTUB5-COF was investigated by initial heating of a sample starting at room temperature to 130 °C and comparing the X-ray diffractograms measured at ambient temperature (**Figure 7**). While the crystallinity decreases in the process, the very similar amorphous diffraction pattern above 210 °C until 270 °C suggests its thermal stability. We obtained the original unit cell via single crystal X-ray diffraction up to 130 °C, suggesting that the basic structure of GTUB5 HOF is thermally stable at 130 °C. Although the XRD data of the original HOF structure is mostly retained up to 190 °C, the single crystal diffraction experiments didn't provide a unit cell for the samples heated above 130°C; due to the significantly decreased crystallinity, no further single crystal diffraction measurements could be followed up. As the heated sample retained its crystalline shape and color under stereo microscope, we tried 3D electron diffraction to identify the structure of the resulting HOF. Still, getting a data set suitable for structural characterization was impossible. The heated crystals of GTUB5-COF break up in muscle pattern, which is generally seen in glass materials. **Figure 7** displays the X-ray diffractograms measured at ambient temperature (20 °C), at 130 °C, at 150 °C, at 170 °C, at 190 °C, at 210 °C, and 270 °C

from 5° to 50° 2θ in comparison to each other. Each time, the same sample was heated for 2h at the respective temperature.

The heated sample of GTUB5-COF was then added to cold water and boiling water for one hour to test its chemical stability. Due to its amorphous structure, it was impossible to confirm whether GTUB5-COF retained its structure. The crystal shape and color stayed stable in the cold and boiled water after 1 h and did not dissolve or dissipate (The overall structure might have experienced phase transfers due to the presence of flexible P-O-P bonds; we were not able to confirm it due to the amorphous nature of the GTUB5-COF). **Figure S6**, *Supporting Information* displays the X-ray diffractograms of the sample measured after 210°C heating, after 1 h in cold water, and the activated sample at 270 °C. Although amorphous at this point, a characteristic diffraction pattern still can be identified, thus suggesting the presence of an intact sample. Furthermore, the constant reproducibility of the water adsorption isotherms for one month also suggests the stability of the reported GTUB5-COF in the presence of water vapor. The water-treated GTUB5-COF at 210 °C and activated GTUB5-COF at 270 °C have similar two broad peaks in their X-ray diffractogram suggesting the thermal stability of the compound. The disappearance of relatively sharper peaks at the water-treated sample at 210 °C also suggests the dissolving of DMA solvents in the pores, which are miscible with water, increasing the amorphous nature of GTUB5-COF after water treatment. Furthermore, MAS-NMR experiments also proved the presence of linkers at 220 °C.

MS-TGA: We coupled thermogravimetric analysis with mass spectrometry to better understand the underlying reaction mechanism. As seen in **Figure 8**, the TGA measurement was performed between 30 °C to 600 °C. The green curve displays the number of H_2O ions detected by mass spectrometry, the dark blue line shows the amount of detected dimethylamine, and the light blue line represents the detected DMF. The first step of the TGA curve can be observed at 50 °C, likely due to the loss of the solvent or guest molecules. A second step is noticeable after 230 °C, which is connected to the detection of dimethylamine by mass spectrometry. This affirms the hypothesis that a condensation reaction involving the deprotonation of the dimethylamine cations and the phosphonic acid groups of GTUB5 took place. The third step, starting at 390 °C, is connected to detecting dimethylamine and DMF by mass spectrometry. At 390 °C, the complete decomposition of the porphyrin core begins. The formation of DMA and DMF at 390 °C may be explained as pyrolysis products observed after the decomposition of the porphyrin residue.

Electrochemical Stability: The reactivity and stability of the GTUB5-COF sample were investigated in a three electrode cell setup with a platinum wire and a Ag/AgCl (3 M) as counter and reference electrodes, respectively. Open circuit potential (OCP) was measured in an aqueous 0.5 M Na_2SO_4 electrolyte for 1 h to evaluate the thermodynamic behavior of the material, followed by linear sweep voltammetry (LSV) in a potential window from -1 V to 2 V vs. Ag/AgCl (3 M) with a scan rates of 1 mV s^{-1} to assess the electrochemical stability window. To perform the experiments, 50 µL of a 0.5 mg mL^{-1} aqueous GTUB5-COF dispersion was drop-casted over a glassy carbon electrode (GCE) with a surface area of 7 mm^2 and dried at room temperature. The OCP measurement illustrated in **Figure 9A** suggests stability of the GTUB5-COF material in aqueous neutral environment, exhibiting a noble and stable E_{OCP} = +0.425 vs. Ag/AgCl, highlighting long-term stability of the material in aqueous electrolytes.[45] The GTUB5-COF was further investigated through LSV, as shown in **Figure 9B**. The material exhibited a electrochemical stability window ranging from -0.6 V to +1.3 V vs. Ag/AgCl followed by an oxidation of the aqueous media.[46] Such behavior suggests potential application in electrochemical systems such as catalysis, combining a layered compact material, as shown in *Supporting information* **Figure S10A-F**, with a desirable electrochemical stability.

Gas sorption: While COFs have shown potential to capture CO_2, there are only a small number of COFs and MOFs that can capture CO_2 in the presence of water vapor, according to a recent comprehensive review article published by Zhao et al.[47-50] To gain more insight into the material and estimate the activation temperature, we performed TGA-MS experiments. According to TGA-MS data, DMA molecules in the pores started to leave the pores at ca. 230 °C. Therefore, unpowdered large needles of GTUB5-COF with sizes between 1 mm and 3 mm were activated by heating to 270°C under vacuum for 2 h to ensure that all of the DMA molecules were evaporated to empty the pores of GTUB5-COF. As seen in Figure 2S, the activated GTUB5-COF at 270 °C, and water-treated GTUB5-COF have a similar amorphous PXRD pattern. Gas sorption measurements were done on the BELSorp-max II by MicrotracBEL Corporation. Each CO_2 and N_2 sorption measurement was repeated three times, and in between each measurement, GTUB5-COF was heated to 60 °C to clear pores from the remaining residual CO_2 and N_2 gases. Water sorption measurements were performed using a Quantachrome V-STAR4. Between each water sorption measurement, GTUB5-COF was heated to 200 °C for 2 h to remove the residual water from GTUB5-COF's pores. Each of the

repeated gas sorption and water sorption measurements provided similar reproducible adsorption isotherms.

Nitrogen sorption measurements at 77 K revealed negligible N_2 adsorption capacity and low surface area for GTUB5-COF, which is below 1 m^2/g according to BET calculations. This might be a result of a phase transfer to a denser structure at low temperatures due to the presence of flexible sp^3 P-O-P linkages in GTUB5-COF. In contrast, GTUB5-COF (unpowdered needles between ca. 1 mm and 3 mm) exhibits notable CO_2 and water vapor uptake at room temperature compared to the N_2 sorption studies. As we used 1-3 mm long needle-shaped GTUB5-COF sample in the measurements, the error that might originate from the presence of fine powder surface area should be minimal. As seen in **Figure 10a**, three different isotherms at 273 K, 283 K, and 293 K were measured for CO_2 adsorption. Much higher CO_2 adsorption compared to nitrogen was observed. The distinct adsorption behavior at different temperatures suggests the dynamic nature of GTUB5-COF's porous structure and potential phase transfers due to the presence of sp^3 linkages in GTUB5-COF. It is kinetically difficult for N_2 to access the pores GTUB5-COF at 77 K. Nevertheless, GTUB5-COF demonstrates that its pores are suitable for CO_2 compared to N_2.

The CO_2 adsorption isotherms showed a distinct hysteresis over the whole pressure range, indicating favorable interaction between adsorbent and adsorbate. The observed hysteresis in **Figure 10b**, closely resembles the characteristic features of type H4, as shown by Sing in 1985.[51] This observation suggests the presence of small and narrow pores with a polar surface. Following the observed hysteresis, the BET calculation derived from the adsorption isotherm at 273 K gave a CO_2-accessible surface area of 47 m^2/g and a total pore volume of 0.014 cm^3/g. We calculated the heat of adsorption for CO_2 adsorption by measuring the CO_2 adsorption at three different temperatures at 273 K, 283 K, and 293 K via fitting the adsorption isotherms by Langmuir-Freundlich model (**Figure S7-S8**, *Supporting Information*) and using the Clausius-Clapeyron equation.[52] The heat of adsorption of CO_2 was calculated to be -27 kJ/mol at a CO_2 loading of 0.01 mmol/g. This value is relatively constant over the observed pressure range.

$$\Delta H_{ads}(n) = -R \cdot ln(p_2/p_1)(T_1 \cdot T_2/(T_2 - T_1)) \quad \text{Eq. 1}$$

As seen in **Figure 10** (right), water vapor sorption measurements at 283 K, 293 K, and 303 K showed an adsorption pattern with a slight convex curvature, exhibiting a type V hysteresis.[51] This observation also confirms the presence of limited porosity and polar pore surfaces. Heat of water adsorption was also calculated using the same method, giving a value

of -21 kJ/mol for a loading of 0.2 mmol/g at a pressure of 10^{-4} bar. The load of 0.2 mmol/g was used due to lower accuracy within the low-pressure region for water sorption and according to the available measure points (**Figure S9**, *Supporting Information*). Unlike CO_2, the heat of adsorption for water vapor becomes more negative with increased pressure. The formation of the hydrogen bonds between adsorbed water molecules probably caused the more favorable change in the heat of adsorption for water. Both CO_2 gas and water vapor show favorable interaction with the pore surface of GTUB5-COF. Comparability to the heat of carbon dioxide adsorption is complicated due to the distinct characteristics inherent to CO_2 gas and water vapor. Nevertheless, more negative -27 kJ/mol heat of adsorption value for CO_2 sorption at lower pressure suggests the potential of GTUB-COF for selective CO_2 capture. Furthermore, the repeated consistency of water adsorption isotherms also proves the stability of GTUB5-COF in water vapor.

Figure 11 depicts the converted Kubelka-Munk spectra of GTUB5-COF derived from its diffuse reflectance. The localized transitions of the porphyrin entities within the COF characterize it. It reveals the characteristic Soret band at around 350 nm and the Q bands between 430 nm and roughly 700 nm. This suggests the presence of an intact porphyrin core in heated GTUB5-COF, which was activated at 270 °C. The compound shows weak broad-banded fluorescence of the porphyrin units in the near infrared range, peaking at around 800 nm.

Conclusions: Herein, we introduce a new family of covalent organic frameworks, pyrophosphonate-COFs. In this report, we present a straightforward and environmentally friendly method to condense phosphonic acid HOF crystals to synthesize pyrophosphonate-COFs in a single step, accomplished by heating the precursor HOF crystals without additional chemical reagents. We used the MAS-NMR, FT-IR, and TGA-MS experiments to monitor the formation of pyrophosphonate bonds in GTUB5-COF. Based on the MS-TGA data, the DMA^+ cations in GTUB5 donate their protons to the parent HOF structure to promote the condensation of phosphonic acid groups. After the condensation of GTUB5 to form GTUB5-COF, the neutral DMA molecules are leaving the GTUB5-COF structure after ca. 230 °C generating void spaces suitable for small molecule capture. The heat of adsorption experiments indicate that GTUB5-COF exhibits higher selectivity for CO_2 molecules compared to the water vapor at lower pressures. In contrast, at higher pressures, it becomes more selective for water vapor. The reported GTUB5-COF exhibits remarkable stability in water and water vapor during the BET measurements, and it is not visually dissolved in cold and boiling

water (dissolved 5,10,15,20-tetrakis[p-phenylphosphonic acid] porphyrin linker produces a very dark red solution).

Furthermore, we have shown that GTUB5-COF is electrochemically stable in 0.5 M Na_2SO_4 electrolyte in water, and MAS-NMR experiments has shown that the linker cores of GTUB5-COF did not chemically decompose at 220 °C. While COF research has yielded diverse families and applications across various fields, a significant and desirable advancement in COF chemistry is the creation of water-stable and CO_2-selective COFs. The presented pyrophosphonate-COF GTUB5-COF in this work may provide the required stability and selectivity in COF field, and it can address the diverse problems and find industrial use. These findings show GTUB5-COF's potential in controlled gas adsorption and selective CO_2 capture, promising new directions in sustainable gas storage and separation. We are currently exploring the full potential of pyrophosphonate-COFs, determining their long-term stability in different media, and using longer tethered arylphosphonic acids to improve the surface areas of pyrophosphonate-COFs.

ASSOCIATED CONTENT

Supporting Information. Details of synthesis, NMR data, FTIR data, SEM pictures, and details of gas sorption studies.

AUTHOR INFORMATION

Corresponding Author

* Gündoğ Yücesan guendog.yuecesan@hhu.de and *Jörn Schmedt auf der Günne gunnej@chemie.uni-siegen.de

Author Contributions

The manuscript was written through contributions of all authors. All authors have given approval to the final version of the manuscript. ‡These authors contributed equally.

Funding Sources

Gündoğ Yücesan and Jens Beckmann would like to thank DFG for funding their research with grant numbers YU 267/2-1 and BE 3716/9-1. M.S. gratefully acknowledges funding by a materials cost allowance of the Fonds der Chemischen Industrie e.V. and financial support by the “Young College” of the North-Rhine Westphalian Academy of Sciences and Arts. X. K., R. O. and T. H. H. S. are equally contributed first authors.

Notes

Any additional relevant notes should be placed here.

ACKNOWLEDGMENTS

X. K., R. O. and T. H. H. S. are equally contributed first authors. TU-Berlin has a patent application protecting the rights of pyrophosphonate-COFs.

ABBREVIATIONS

COF, covalent organic framework; HOF, hydrogen bonded organic framework; MOF, metal organic framework; MS-TGA, mass spectroscopy coupled thermogravimetric analysis; MAS NMR, magic angle spinning nuclear magnetic resonance; SEM, scanning electron microscopy; OCP, open circuit potential; LSV, linear sweep voltammetry; STP, standard temperature and pressure; V_a, Volume adsorbed.

REFERENCES

(1) El-Kaderi, H. M.; Hunt, J. R.; Mendoza-Cortés, J. L.; Côté, A. P.; Taylor, R. E.; O'Keeffe, M.; Yaghi, O. M. Designed Synthesis of 3D Covalent Organic Frameworks. *Science* **2007**, *316*, 268.
(2) Côté, A. P.; Benin, A. I.; Ockwig, N. W.; Keeffe, M.; Matzger, A. J.; Yaghi, O. M. Porous, Crystalline, Covalent Organic Frameworks. *Science* **2005**, *310* (5751), 1166. DOI: 10.1126/science.1120411.
(3) Lin, R.-B.; He, Y.; Li, P.; Wang, H.; Zhou, W.; Chen, B. Multifunctional porous hydrogen-bonded organic framework materials. *Chemical Society Reviews* **2019**, *48* (5), 1362-1389, 10.1039/C8CS00155C. DOI: 10.1039/C8CS00155C.
(4) Côté, A. P.; Benin, A. I.; Ockwig, N. W.; O'Keeffe, M.; Matzger, A. J.; Yaghi, O. M. Porous, Crystalline, Covalent Organic Frameworks. *Science* **2005**, *310*, 1166.
(5) Qian, C.; Qi, Q. Y.; Jiang, G. F.; Cui, F. Z.; Tian, Y.; Zhao, X. Toward Covalent Organic Frameworks Bearing Three Different Kinds of Pores: The Strategy for Construction and COF-to-COF Transformation via Heterogeneous Linker Exchange. *J. Am. Chem. Soc.* **2017**, *139*, 6736.
(6) Geng, K.; He, T.; Liu, R.; Dalapati, S.; Tan, K. T.; Li, Z.; Tao, S.; Gong, Y.; Jiang, Q.; Jiang, D. Covalent Organic Frameworks: Design, Synthesis, and Functions. *Chemical Reviews* **2020**, *120* (16), 8814-8933. DOI: 10.1021/acs.chemrev.9b00550.
(7) Lohse, M. S.; Bein, T. Covalent Organic Frameworks: Structures, Synthesis, and Applications. *Adv. Funct. Mater.* **2018**, *28*, 1705553.
(8) Segura, J. L.; Mancheno, M. J.; Zamora, F. Covalent Organic Frameworks Based on Schiff-Base Chemistry: Synthesis, Properties and Potential Applications. *Chem. Soc. Rev.* **2016**, *45*, 5635.
(9) Han, X.-H.; Gong, K.; Huang, X.; Yang, J.-W.; Feng, X.; Xie, J.; Wang, B. Syntheses of Covalent Organic Frameworks via a One-Pot Suzuki Coupling and Schiff's Base Reaction for C2H4/C3H6 Separation. *Angewandte Chemie International Edition* **2022**, *61* (25), e202202912, https://doi.org/10.1002/anie.202202912. DOI: https://doi.org/10.1002/anie.202202912 (acccessed 2023/04/07).
(10) Abuzeid, H. R.; El-Mahdy, A. F. M.; Kuo, S.-W. Covalent organic frameworks: Design principles, synthetic strategies, and diverse applications. *Giant* **2021**, *6*, 100054. DOI: https://doi.org/10.1016/j.giant.2021.100054.
(11) Han, S. S.; Furukawa, H.; Yaghi, O. M.; Goddard, W. A. Covalent Organic Frameworks as Exceptional Hydrogen Storage Materials. *J. Am. Chem. Soc.* **2008**, *130*, 11580.
(12) Doonan, C. J.; Tranchemontagne, D. J.; Glover, T. G.; Hunt, J. R.; Yaghi, O. M. Exceptional Ammonia Uptake by a Covalent Organic Framework. *Nat. Chem.* **2010**, *2*, 235.
(13) Furukawa, H.; Yaghi, O. M. Storage of Hydrogen, Methane, and Carbon Dioxide in Highly Porous Covalent Organic Frameworks for Clean Energy Applications. *J. Am. Chem. Soc.* **2009**, *131*, 8875.
(14) Cai, S. L.; Zhang, Y. B.; Pun, A. B.; He, B.; Yang, J. H.; Toma, F. M.; Sharp, I. D.; Yaghi, O. M.; Fan, J.; Zheng, S. R.; et al. Tunable Electrical Conductivity in Oriented Thin Films of Tetrathiafulvalene-Based Covalent Organic Framework. *Chem. Sci.* **2014**, *5*, 4693.
(15) Klontzas, E.; Tylianakis, E.; Froudakis, G. E. Designing 3D COFs with Enhanced Hydrogen Storage Capacity. *Nano Lett.* **2010**, *10*, 452.
(16) Liu, S.; Yao, L.; Lu, Y.; Hua, X.; Liu, J.; Yang, Z.; Wei, H.; Mai, Y. All-Organic Covalent Organic Framework/Polyaniline Composites as Stable Electrode for High-Performance Supercapacitors. *Mater. Lett.* **2019**, *236*, 354.

(17) Tholen, P.; Peeples, C. A.; Schaper, R.; Bayraktar, C.; Erkal, T. S.; Ayhan, M. M.; Çoşut, B.; Beckmann, J.; Yazaydin, A. O.; Wark, M.; et al. Semiconductive microporous hydrogen-bonded organophosphonic acid frameworks. *Nat Commun* **2020**, *11* (1), 3180. DOI: 10.1038/s41467-020-16977-0.
(18) Tholen, P.; Peeples, C. A.; Ayhan, M. M.; Wagner, L.; Thomas, H.; Imbrasas, P.; Zorlu, Y.; Baretzky, C.; Reineke, S.; Hanna, G.; Yücesan, G. Tuning Structural and Optical Properties of Porphyrin-based Hydrogen-Bonded Organic Frameworks by Metal Insertion. *Small* **2022**, *18* (49), 2204578, https://doi.org/10.1002/smll.202204578. DOI: https://doi.org/10.1002/smll.202204578 (acccessed 2022/12/12).
(19) Jeffrey, G. A. *An Introduction to Hydrogen Bonding*; 1997.
(20) Sun, Y.; Wei, J.; Fu, Z.; Zhang, M.; Zhao, S.; Xu, G.; Li, C.; Zhang, J.; Zhou, T. Bio-Inspired Synthetic Hydrogen-Bonded Organic Frameworks for Efficient Proton Conduction. *Advanced Materials* **2023**, *35* (7), 2208625. DOI: https://doi.org/10.1002/adma.202208625 (acccessed 2023/08/31).
(21) Harsági, N.; Keglevich, G. The Hydrolysis of Phosphinates and Phosphonates: A Review. In *Molecules*, 2021; Vol. 26.
(22) Dürr-Mayer, T.; Qiu, D.; Eisenbeis, V. B.; Steck, N.; Häner, M.; Hofer, A.; Mayer, A.; Siegel, J. S.; Baldridge, K. K.; Jessen, H. J. The chemistry of branched condensed phosphates. *Nature Communications* **2021**, *12* (1), 5368. DOI: 10.1038/s41467-021-25668-3.
(23) Schütrumpf, A.; Kirpi, E.; Bulut, A.; Morel, F. L.; Ranocchiari, M.; Lork, E.; Zorlu, Y.; Grabowsky, S.; Yücesan, G.; Beckmann, J. Tetrahedral Tetraphosphonic Acids. New Building Blocks in Supramolecular Chemistry. *Crystal Growth & Design* **2015**, *15* (10), 4925-4931. DOI: 10.1021/acs.cgd.5b00811.
(24) Heggen, B.; Roy, S.; Müller-Plathe, F. Ab Initio Calculations of the Condensation of Phosphonic Acid and Methylphosphonic Acid: Chemical Properties of Potential Electrolyte Materials for Fuel Cell Applications. *The Journal of Physical Chemistry C* **2008**, *112* (36), 14209-14215. DOI: 10.1021/jp803589w.
(25) Zhang, C.; Turner, A. M.; Wang, J.; Marks, J. H.; Fortenberry, R. C.; Kaiser, R. I. Low-Temperature Thermal Formation of the Cyclic Methylphosphonic Acid Trimer [c-(CH3PO2)3]. *ChemPhysChem* **2023**, *24* (4), e202200660. DOI: https://doi.org/10.1002/cphc.202200660 (acccessed 2023/09/07).
(26) Yucesan, G.; Ouellette, W.; Golub, V.; O'Connor, C. J.; Zubieta, J. Solid state coordination chemistry: temperature dependence of the crystal chemistry of the oxovanadium-phenylphosphonate-copper(II)-2,2'-bipyridine system. Crystal structures of the one-dimensional [{Cu(bpy)}VO2(O3PC6H5)(HO3PC6H5)], [{Cu3(bpy)3(H2O)}V4O9(O3PC6H5)4], [{Cu(bpy)}2V3O6(O3PC6H5)3(HO3PC6H5)] and [{Cu(bpy)}VO(O3PC6H5)2]. *Solid State Sciences* **2005**, *7* (4), 445-458. DOI: https://doi.org/10.1016/j.solidstatesciences.2005.01.009.
(27) Guo, L.-R.; Bao, S.-S.; Li, Y.-Z.; Zheng, L.-M. Ag(i)-mediated formation of pyrophosphonate coupled with C–C bond cleavage of acetonitrile. *Chemical Communications* **2009**, (20), 2893-2895, 10.1039/B902162K. DOI: 10.1039/B902162K.
(28) Guo, L.-R.; Tong, J.-W.; Liang, X.; Köhler, J.; Nuss, J.; Li, Y.-Z.; Zheng, L.-M. Silver(i) pyrophosphonates: structural, photoluminescent and thermal expansion studies. *Dalton Transactions* **2011**, *40* (24), 6392-6400, 10.1039/C1DT10236B. DOI: 10.1039/C1DT10236B.
(29) Arz, M. I.; Annibale, V. T.; Kelly, N. L.; Hanna, J. V.; Manners, I. Ring-Opening Polymerization of Cyclic Phosphonates: Access to Inorganic Polymers with a PV–O Main Chain. *Journal of the American Chemical Society* **2019**, *141* (7), 2894-2899. DOI: 10.1021/jacs.8b13435.

(30) Tholen, P.; Peeples, C. A.; Schaper, R.; Bayraktar, C.; Erkal, T. S.; Ayhan, M. M.; Cosut, B.; Beckmann, J.; Yazaydin, A. O.; Wark, M.; et al. Semiconductive microporous hydrogen-bonded organophosphonic acid frameworks. *Nat. Commun.* **2020**, *11*, 3180.
(31) Schülke, U.; Kayser, R.; Neumann, P. Zur Darstellung von Cyclophosphaten, Cyclophosphatophosphonaten, Diphosphonaten und Diphosphiten in Harnstoffschmelzen. *Zeitschrift für anorganische und allgemeine Chemie* **1989**, *576* (1), 272-280. DOI: https://doi.org/10.1002/zaac.19895760131 (acccessed 2023/12/05).
(32) Ohms, G.; Großmann, G.; Schwab, B.; Schiefer, H. SYNTHESIS AND 31P AND 13C NMR STUDIES OF PYROPHOSPHONIC ACIDS. *Phosphorus, Sulfur, and Silicon and the Related Elements* **1992**, *68* (1-4), 77-89. DOI: 10.1080/10426509208038374.
(33) Hartmann, P.; Vogel, J.; Schnabel, B. The Influence of Short-Range Geometry on the 31P Chemical-Shift Tensor in Protonated . Phosphates. *Journal of Magnetic Resonance, Series A* **1994**, *111* (1), 110-114. DOI: https://doi.org/10.1006/jmra.1994.1234.
(34) Iuga, A.; Ader, C.; Gröger, C.; Brunner, E. Applications of Solid-State 31P NMR Spectroscopy. In *Annual Reports on NMR Spectroscopy*, Webb, G. A. Ed.; Vol. 60; Academic Press, 2006; pp 145-189.
(35) Demadis, K. D.; Katarachia, S. D.; Koutmos, M. Crystal growth and characterization of zinc–(amino-tris-(methylenephosphonate)) organic–inorganic hybrid networks and their inhibiting effect on metallic corrosion. *Inorganic Chemistry Communications* **2005**, *8* (3), 254-258. DOI: https://doi.org/10.1016/j.inoche.2004.12.019.
(36) Demadis, K. D.; Katarachia, S. D.; Raptis, R. G.; Zhao, H.; Baran, P. Alkaline Earth Metal Organotriphosphonates: Inorganic−Organic Polymeric Hybrids from Dication−Dianion Association. *Crystal Growth & Design* **2006**, *6* (4), 836-838. DOI: 10.1021/cg0506368.
(37) Burck, S.; Götz, K.; Kaupp, M.; Nieger, M.; Weber, J.; Schmedt auf der Günne, J.; Gudat, D. Diphosphines with Strongly Polarized P−P Bonds: Hybrids between Covalent Molecules and Donor−Acceptor Adducts with Flexible Molecular Structures. *Journal of the American Chemical Society* **2009**, *131* (30), 10763-10774. DOI: 10.1021/ja903156p.
(38) Schmedt auf der Günne, J. Distance measurements in spin-1/2 systems by 13C and 31P solid-state NMR in dense dipolar networks. *Journal of Magnetic Resonance* **2003**, *165* (1), 18-32. DOI: https://doi.org/10.1016/S1090-7807(03)00242-8.
(39) Luschtinetz, R.; Seifert, G.; Jaehne, E.; Adler, H.-J. P. Infrared Spectra of Alkylphosphonic Acid Bound to Aluminium Surfaces. *Macromolecular Symposia* **2007**, *254* (1), 248-253. DOI: https://doi.org/10.1002/masy.200750837 (acccessed 2023/12/05).
(40) Illy, N.; Couture, G.; Auvergne, R.; Caillol, S.; David, G.; Boutevin, B. New prospects for the synthesis of N-alkyl phosphonate/phosphonic acid-bearing oligo-chitosan. *RSC Advances* **2014**, *4* (46), 24042-24052, 10.1039/C4RA02501F. DOI: 10.1039/C4RA02501F.
(41) Vega, A.; Thissen, P.; Chabal, Y. J. Environment-Controlled Tethering by Aggregation and Growth of Phosphonic Acid Monolayers on Silicon Oxide. *Langmuir* **2012**, *28* (21), 8046-8051. DOI: 10.1021/la300709n.
(42) Thissen, P.; Valtiner, M.; Grundmeier, G. Stability of Phosphonic Acid Self-Assembled Monolayers on Amorphous and Single-Crystalline Aluminum Oxide Surfaces in Aqueous Solution. *Langmuir* **2010**, *26* (1), 156-164. DOI: 10.1021/la900935s.
(43) Turner, A. M.; Abplanalp, M. J.; Blair, T. J.; Dayuha, R.; Kaiser, R. I. An Infrared Spectroscopic Study Toward the Formation of Alkylphosphonic Acids and Their Precursors in Extraterrestrial Environments. *The Astrophysical Journal Supplement Series* **2018**, *234* (1), 6. DOI: 10.3847/1538-4365/aa9183.
(44) Moedritzer, K. Synthesis and Properties of Phosphinic and Phosphonic Acid Anhydrides. *J. Am. Chem. Soc.* **1961**, *83* (21), 4381.

(45) del Olmo, D.; Pavelka, M.; Kosek, J. Open-Circuit Voltage Comes from Non-Equilibrium Thermodynamics. **2021**, *46* (1), 91-108. DOI: doi:10.1515/jnet-2020-0070 (acccessed 2024-01-26).
(46) Liu, M.; Yang, S.; Yang, X.; Cui, C.-X.; Liu, G.; Li, X.; He, J.; Chen, G. Z.; Xu, Q.; Zeng, G. Post-synthetic modification of covalent organic frameworks for CO2 electroreduction. *Nature Communications* **2023**, *14* (1), 3800. DOI: 10.1038/s41467-023-39544-9.
(47) Lin, J.-B.; Nguyen Tai, T. T.; Vaidhyanathan, R.; Burner, J.; Taylor Jared, M.; Durekova, H.; Akhtar, F.; Mah Roger, K.; Ghaffari-Nik, O.; Marx, S.; et al. A scalable metal-organic framework as a durable physisorbent for carbon dioxide capture. *Science* **2021**, *374* (6574), 1464-1469. DOI: 10.1126/science.abi7281 (acccessed 2022/02/25).
(48) Boyd, P. G.; Chidambaram, A.; García-Díez, E.; Ireland, C. P.; Daff, T. D.; Bounds, R.; Gładysiak, A.; Schouwink, P.; Moosavi, S. M.; Maroto-Valer, M. M.; et al. Data-driven design of metal–organic frameworks for wet flue gas CO2 capture. *Nature* **2019**, *576* (7786), 253-256. DOI: 10.1038/s41586-019-1798-7.
(49) Li, H.; Dilipkumar, A.; Abubakar, S.; Zhao, D. Covalent organic frameworks for CO2 capture: from laboratory curiosity to industry implementation. *Chemical Society Reviews* **2023**, *52* (18), 6294-6329, 10.1039/D2CS00465H. DOI: 10.1039/D2CS00465H.
(50) Zeng, Y.; Zou, R.; Zhao, Y. Covalent Organic Frameworks for CO2 Capture. *Adv. Mater.* **2016**, *28*, 2855.
(51) Sing, K. S. W. Reporting physisorption data for gas/solid systems with special reference to the determination of surface area and porosity (Recommendations 1984). **1985**, *57* (4), 603-619. DOI: doi:10.1351/pac198557040603 (acccessed 2023-12-05).
(52) Nuhnen, A.; Janiak, C. A practical guide to calculate the isosteric heat/enthalpy of adsorption via adsorption isotherms in metal–organic frameworks, MOFs. *Dalton Transactions* **2020**, *49* (30), 10295-10307, 10.1039/D0DT01784A. DOI: 10.1039/D0DT01784A.

Schemes and Figures

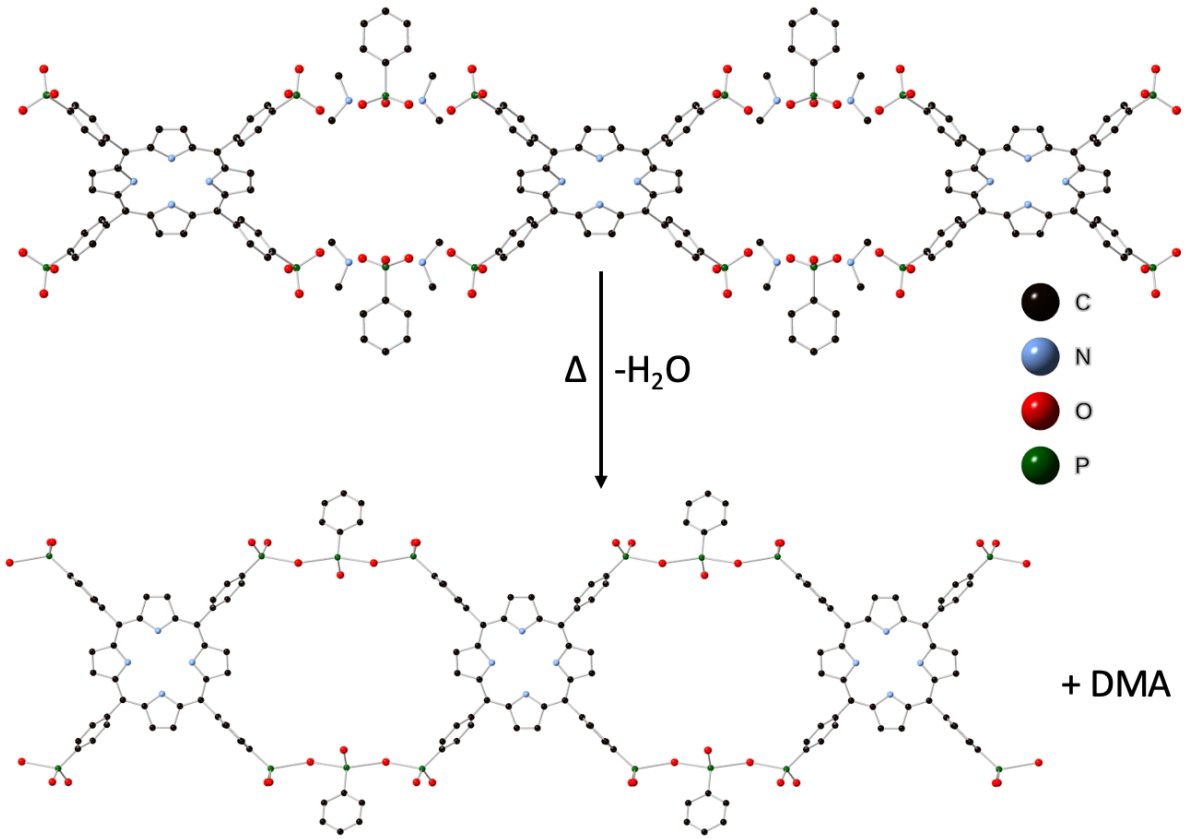

Scheme 1. Synthesis route for forming the proposed pyrophosphonate-COF GTUB5-COF (idealized structure) from GTUB5 via partial condensation of phosphonic acid groups.

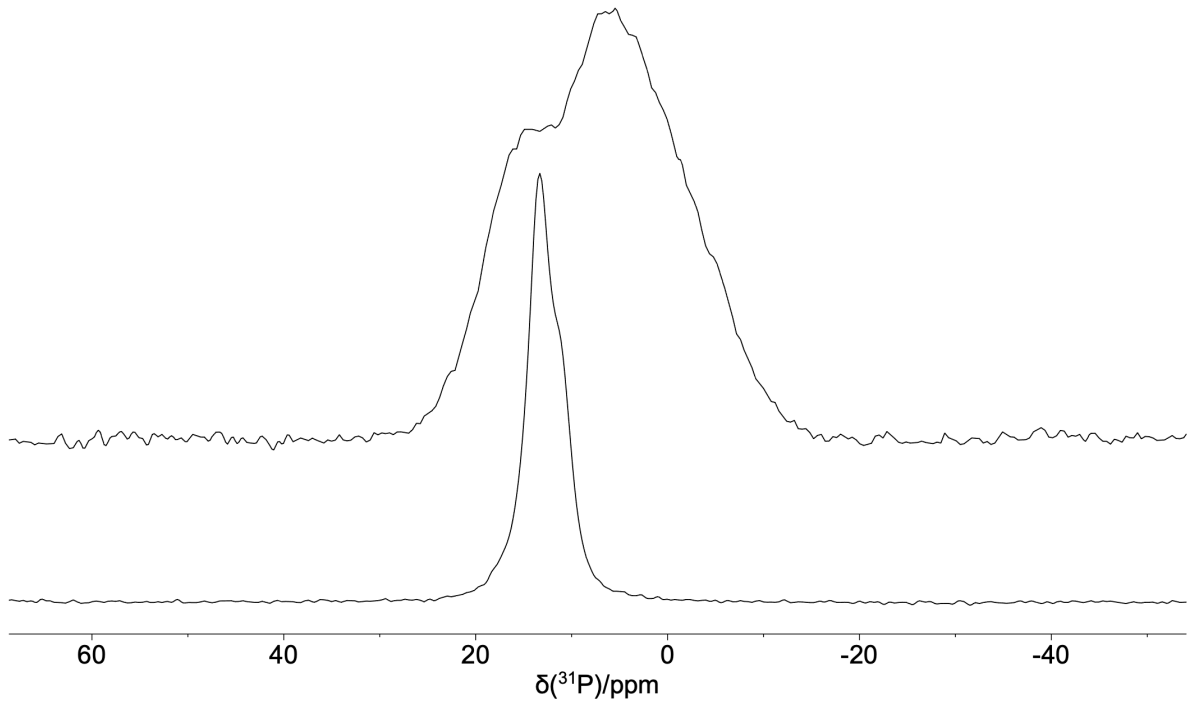

Figure 1. The ^{31}P MAS NMR spectra of the (upper) GTUB5 after anealing at 220 °C spinning at ν_r = 20 kHz, measured with a 7.04 T magnet and (lower) GTUB5 spinning at ν_r = 50 kHz, measured with a 14.1 T magnet.

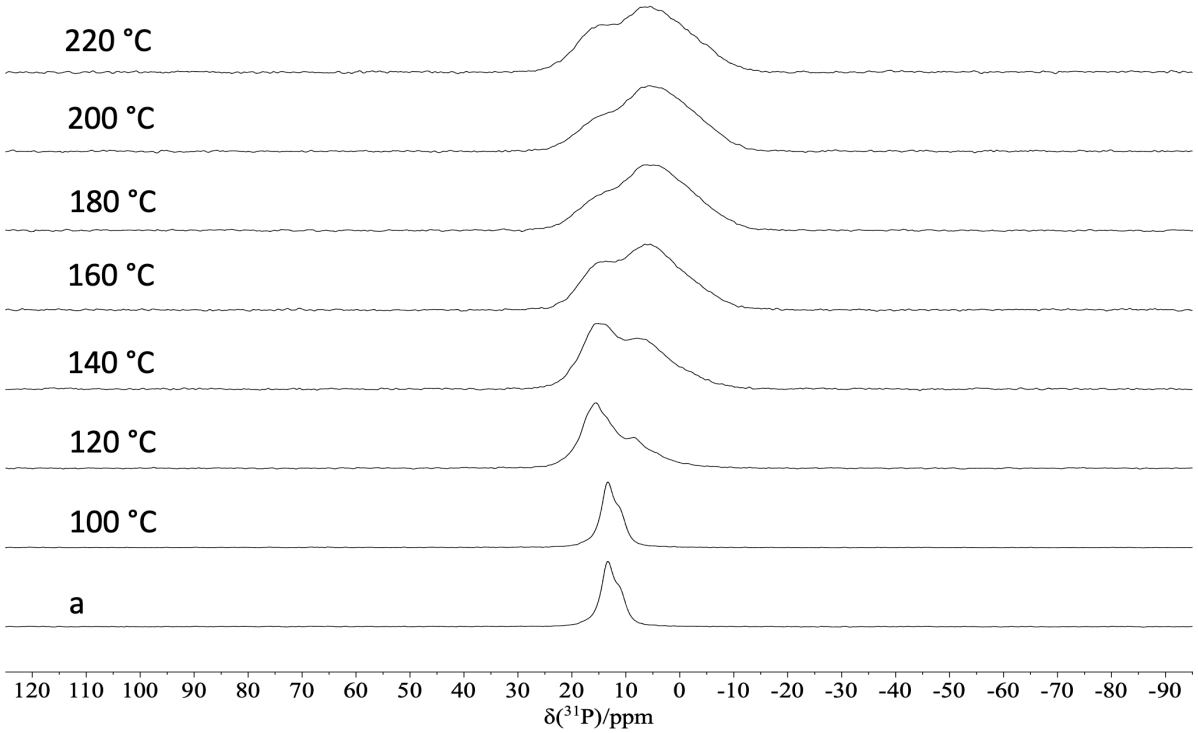

Figure 2. A stack plot of 31P MAS NMR spectra of the sample (a) GTUB5, GTUB5 annealed at (b) 100 °C, (c) 120 °C, (d) 140 °C, (e) 160 °C, (f) 180 °C, (g) 200 °C, and (h) 220 °C. The measurements were performed with a 2.5 mm rotor spinning at 20 kHz under a 7.04 T magnet.

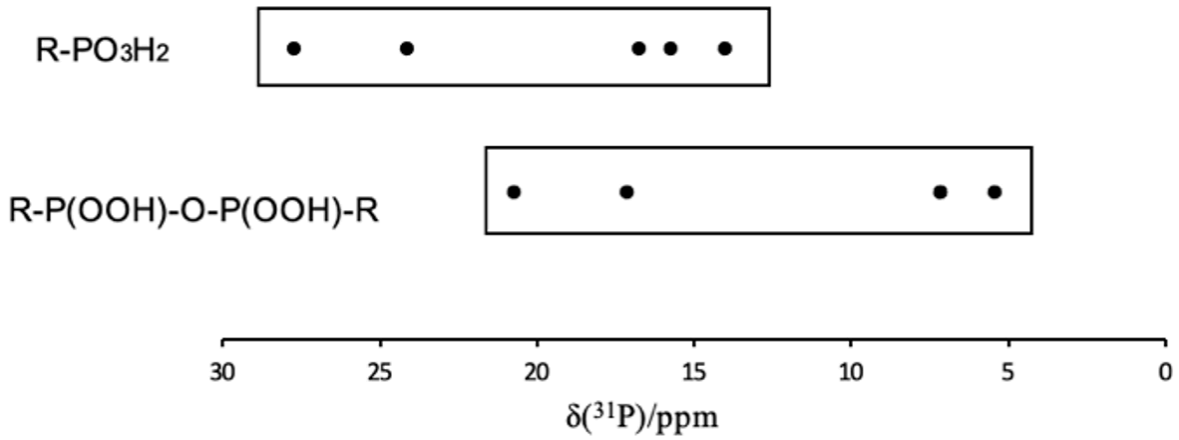

Figure 3. The bar chart which indicates the range of the chemical shift of a hydrogenphosphonate (top)[28] and that of the corresponding pyrophosphonate (bottom).

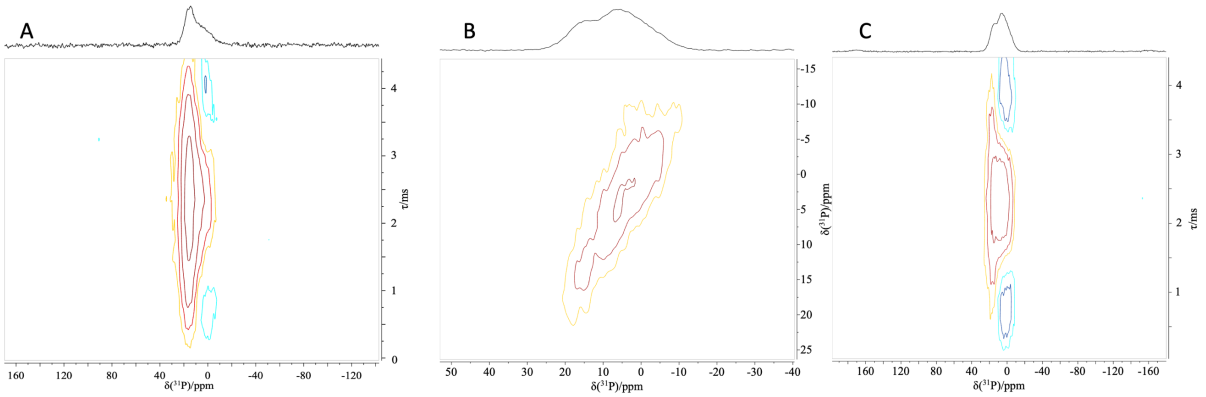

Figure 4. a) The ^{31}P double-quantum constant-time (DQCT) MAS NMR spectrum of the sample GTUB5 after annealing at 220 °C. The phase-adapted PostC7 pulse sequence was used at a spinning frequency of vr = 14286 Hz with a 7.04 T magnet. The total mixing time was 4.48 ms. **b) .** The ^{31}P double-quantum MAS NMR spectrum of the sample GTUB5 after annealing at 220 °C. The spectrum shows that the two peaks at 5 ppm and 14.8 ppm do not have cross correlation. **c)** The ^{31}P double-quantum constant-time (DQCT) MAS NMR spectrum of the sample GTUB5 after annealing at 220 °C. The phase-adapted PostC7 pulse sequence was used at a spinning frequency of vr = 14286 Hz with a 7.04 T magnet. The total mixing time was 4.48 ms.[31, 32]

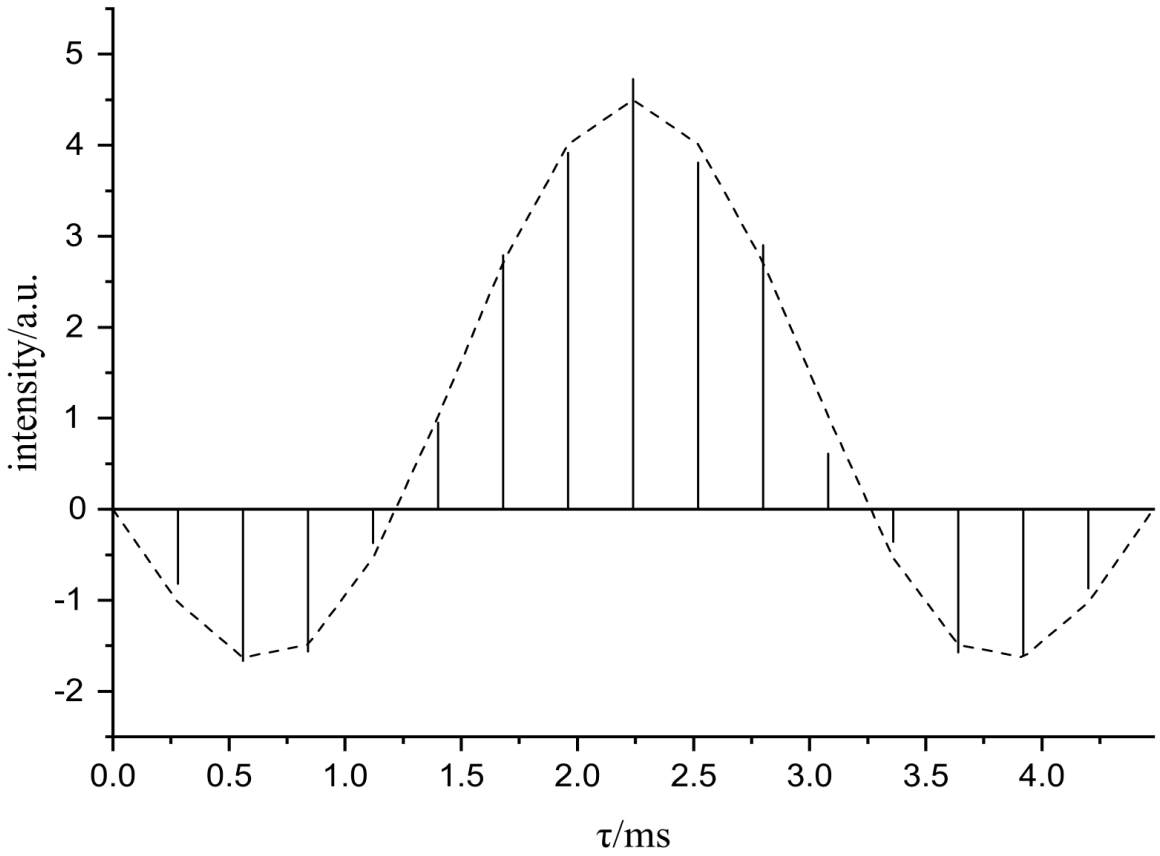

Figure 5. The fitted plot of the ^{31}P double-quantum constant-time build-up NMR curve of the pyrophosphonate peak (peak A, **Table 2**) of the sample GTUB-5 after annealing at 230 °C. The droplines are the experimental data while the dashed line indicates the fitted data. The phase-adapted PostC7 pulse sequence was used at a spinning frequency of ν_r = 14286 Hz. 240 C-elements accumulating 256 transients/FID make up the constant-conversion period.[31, 32]

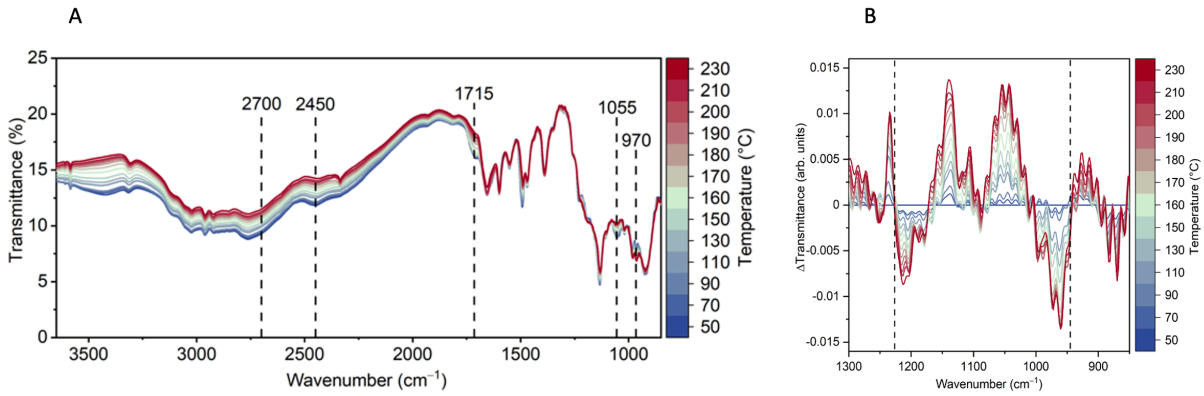

Figure 6. (left) FTIR spectra of HOF GTUB5 during the heating up to 230 °C. (right) FTIR difference spectra of GTUB5 during the heating.

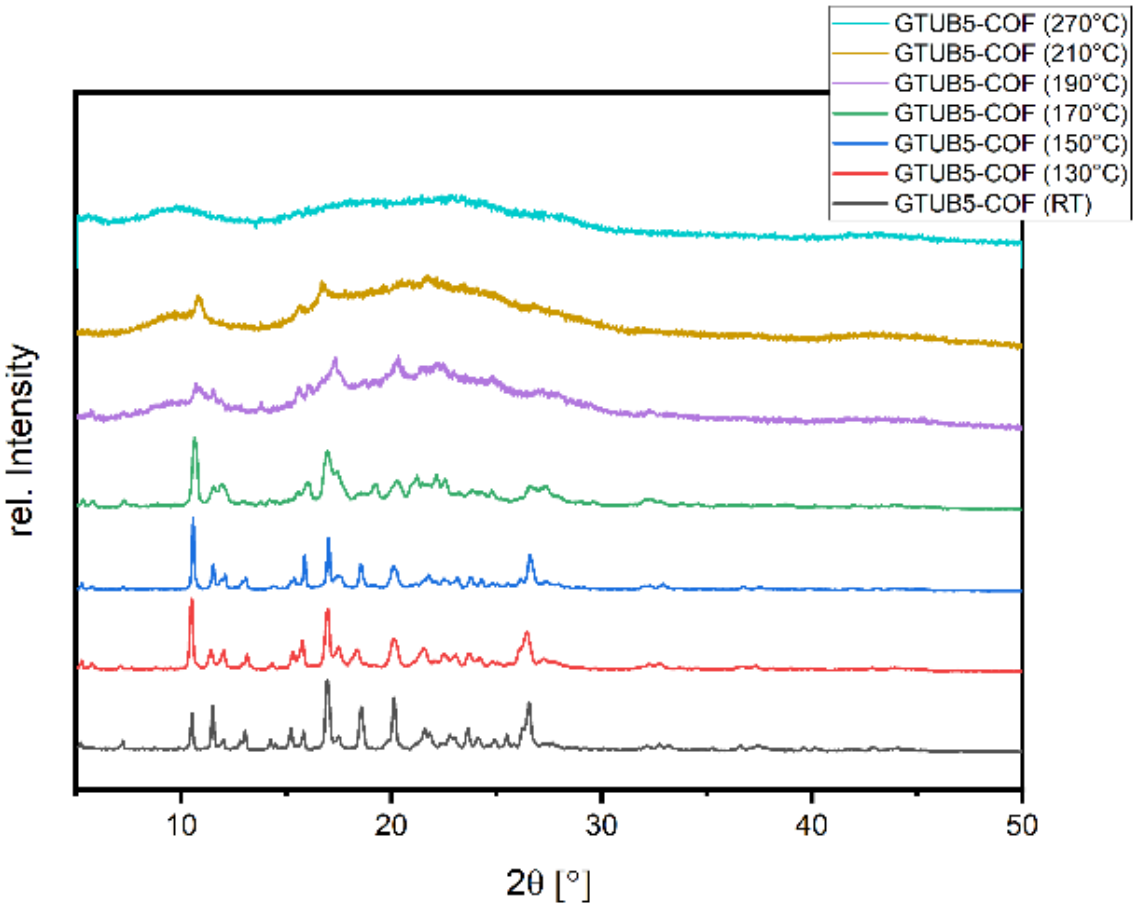

Figure 7: X-ray diffractograms measured from 5° to 50° 2θ for GTUB5 at room temperature (20 °C) and heated for 2 h each time at 130 °C, 150 °C, 170 °C, 190 °C, 210 °C, and 270 °C to show the transition as pyrophosphonate bonds form.

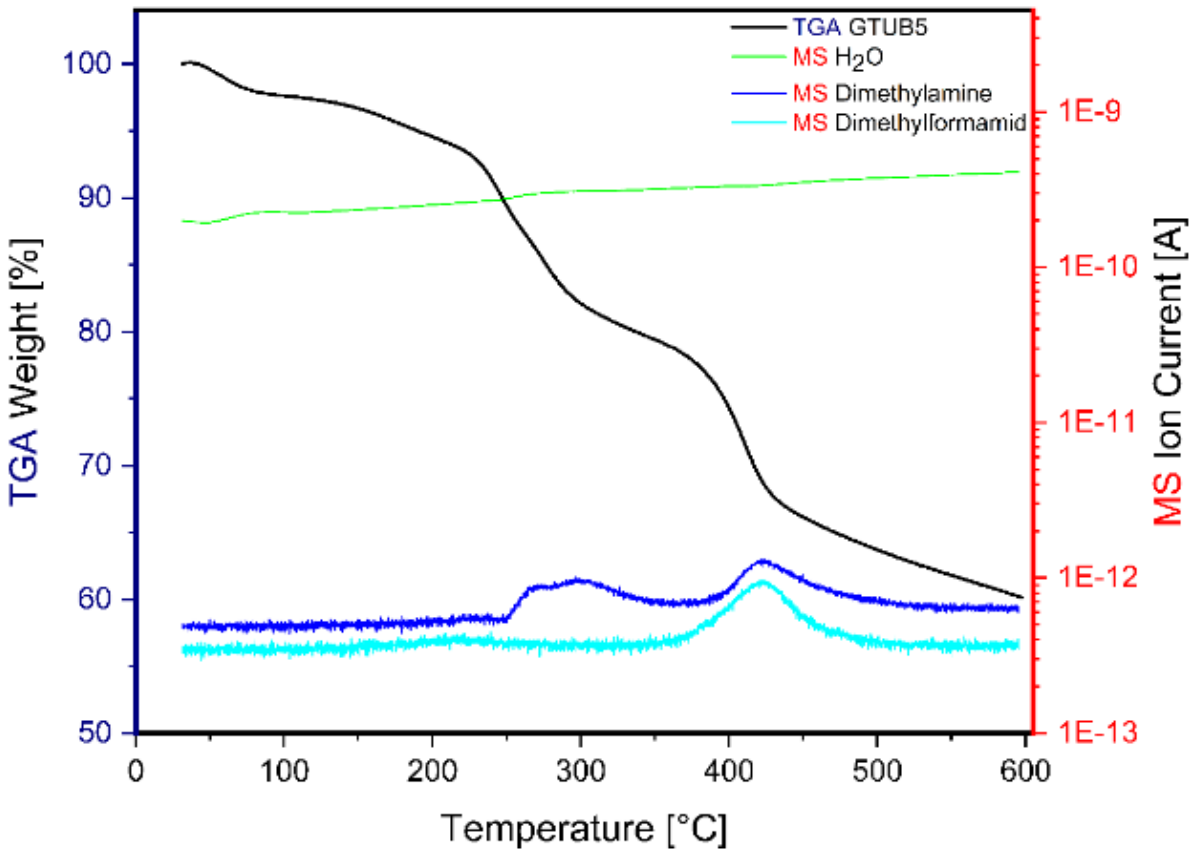

Figure 8. Thermogravimetric analysis and mass spectrometry (H_2O, dimethylamine, and dimethylformamid) curves measured from 30 °C to 600 °C under nitrogen atmosphere at a 10 K/min heating rate for GTUB5.

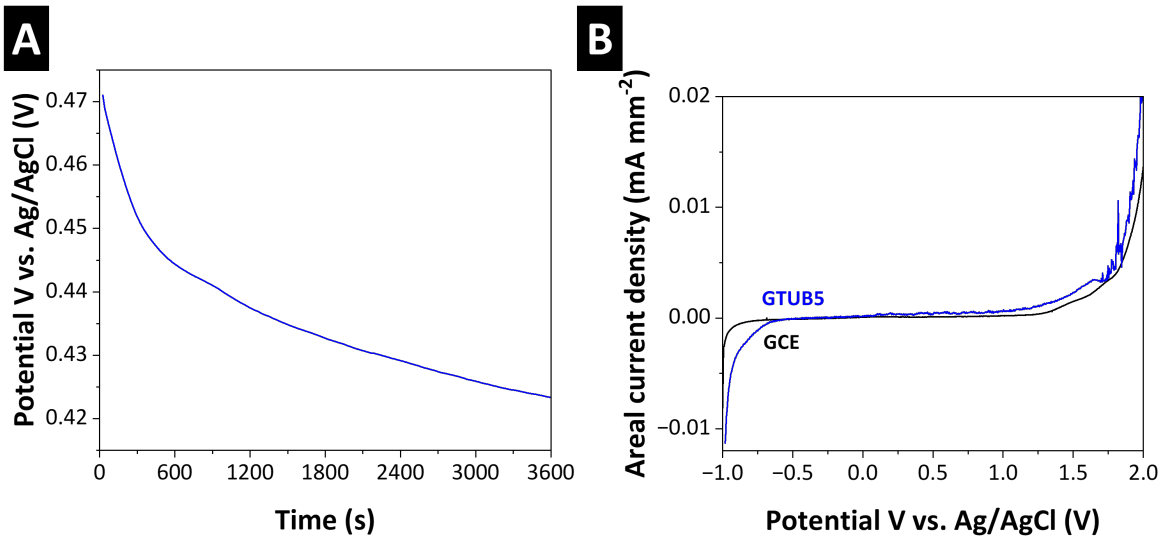

Figure 9. Electrochemical stability of the activated GTUB5-COF sample A) Open circuit potential (OCP) measurement for 1 h and B) Linear sweep voltammogram recorded at 1 mV s^{-1}in aqueous 0.5 M Na_2SO_4 electrolyte.

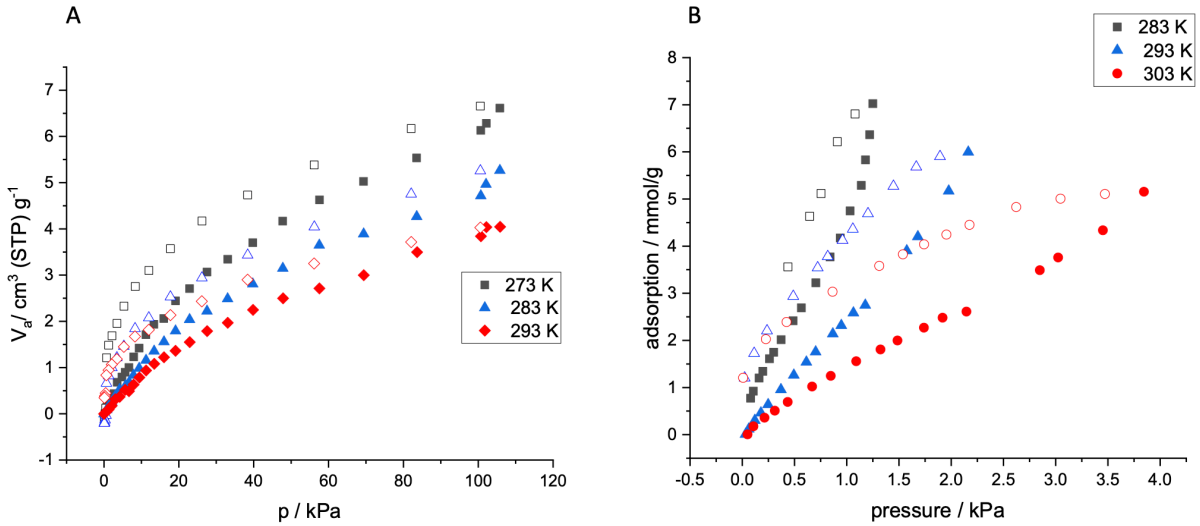

Figure 10. **a**) CO_2 sorption at different temperatures (filled adsorption, empty desorption) **b**) water sorption isotherms at 283 K, 293 K, and 303 K (filled adsorption, empty desorption).

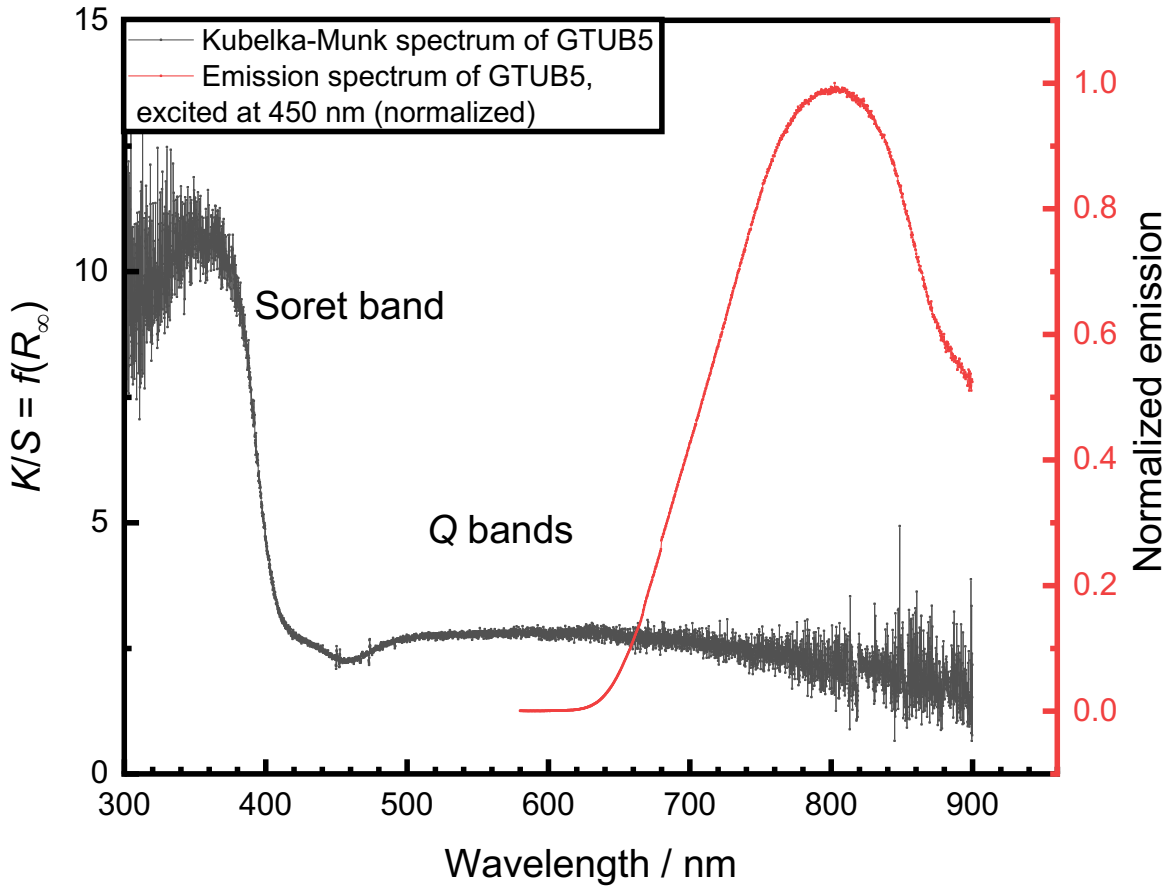

Figure 11. Kubelka-Munk spectrum (black) as derived from diffuse reflectance spectra at room temperature and emission spectrum (excited at 450 nm) of GTUB5 crystals heated at 270 °C.

Tables

Table 1. The result of the SIMPSON simulation and deconvolution of the ^{31}P MAS NMR spectrum on the sample GTUB5 heated at 230 °C. Peak A.

	Peak A	Peak B
δ_{iso}/ppm	14.8	5.0
δ_{xx}/ppm	67.8	89.4
δ_{yy}/ppm	28.5	13.1
δ_{zz}/ppm	-52.0	-87.4
δ_{aniso}/ppm	-66.8	-92.4
η	0.59	0.83

Table 2. The ^{31}P chemical shift values of a series of phosphonic acids and pyrophosphate.

	R-PO_3H_2 [28]	R-P(OOH)-O-P(OOH)-R [29]
R	δ_{iso}/ppm	δ_{iso}/ppm
Ph	15.7	7.1
$PhCH_2$	24.1	17.1
$PhCH_2CH_2$	27.7	20.7
PhCH=CH	16.7	7.1
$PhC(CH_2)$	14.0	5.4